NEW HIGH RESOLUTION MAGNETIC FIELD MODELS AT THE SURFACE OF THE MOON FROM LUNAR PROSPECTOR ALONG-TRACK VECTOR GRADIENTS. D. Ravat[1], M. E. Purucker[2], N. Olsen[3], [1]University of Kentucky, (Dept. of Earth & Environmental Sciences, Lexington, KY 40506, dhananjay.ravat@uky.edu), [2]NASA-GSFC (Planetary Magnetospheres Lab, Code 695, GSFC, MD 20771, michael.e.purucker@nasa.gov), DTU Space (2800 Kgs. Lyngby, Denmark, nio@space.dtu.dk)

Introduction: Results from different combinations of vector and vector gradients (along-track differences) from Lunar Prospector (LP) and SELENE/Kaguya (S/K) spacecrafts suggest that the use of LP vector gradients data alone leads to the best quality crustal magnetic field models at the surface of the Moon using global and local sets of equivalent sources (monopoles) [1, 2]. We use the scheme of iteratively reweighted least squares to account for non-Gaussian data errors. The amplitudes of the monopoles are determined by minimizing the misfit to the components together with the average of |Br| at the ellipsoid surface (i.e. applying a L1 model regularization of |Br|). When vector fields are used, external field contamination leads to spurious N-S features in the downward continued field models even with stringent data selection criteria and ad-hoc noise removal techniques (e.g., selection criteria of satellite's position in the Moon's wake w.r.t. the solar wind and in the Earth's magnetotail, internal/external dipoles fields removal, and ad-hoc low-order polynomial removal, equivalent source based cross-validation of nearby passes, and visual removal of remaining anomalous segments).

In our present effort, we excluded S/K spacecraft data because orbital positioning of the extended mission (low-altitude) suffers from positioning inaccuracies of several meters to kilometers [3]. When better extended mission S/K orbits are available, we will attempt to improve models in and near the South Pole – Aitken (SPA) basin where low altitude S/K data are available.

In the region of Von Kármán crater in the SPA basin, the landing site of Chang'E-4, our high resolution local models show greater detail than global models of the magnetic field of the Moon.

Global Models: We derived global models using only LP along-track gradients with 35000 1° equal-area-spacing monopoles in a single subset and 100000 monopoles (0.66° spacing) in 84 overlapping subsets (Figure 1). Regularization parameters were derived based on visual stable appearance of the fields at the surface of the ellipsoid representing the Moon. In general, the optimum regularization parameter depends on the level of noise in the data as well as the monopole spacing. In regions of high amplitude, high S/N ratio magnetic fields such as Reiner Gamma swirl, we can obtain localized models with higher resolution.

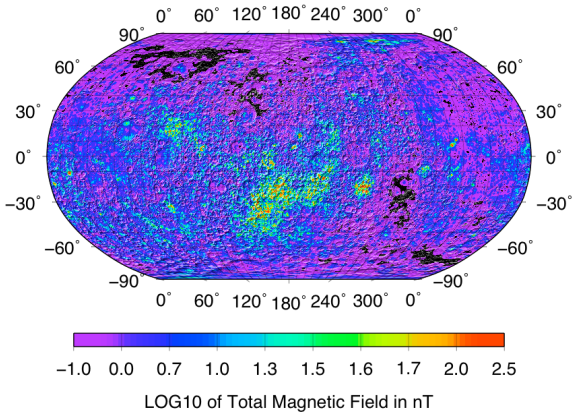

Figure 1. Total field model at the surface of the Moon from monopoles model constrained with L1 regularization (0.66° or 20 km spacing and equivalent monopoles placed at 20 km depth). Note the logarithmic scale of the anomalies to emphasize small amplitude features. The map shows extensive strong magnetic fields in the SPA basin (central part of the map) and localized anomaly features associated with melt sheets within impact craters, other near-surface to deep geologic sources and possibly large impact ejecta formed during the epoch of a strong core field dynamo.

High Resolution Magnetic Field Over Von Kármán Region: To examine in detail the region of Von Kármán crater in the SPA basin – the site of China's Chang'E-4 lander (45.5°S, 177.6°E), we attempted several combinations of monopoles with different spacing and depths. Our highest resolution stable L1 regularized magnetic field model for the region is derived from the low altitude LP gradient data with 6 km spaced monopoles at 5 km depth. We compare this model to the previous high resolution model derived from the method of Surface Vector Mapping (SVM) using Cauchy boundary conditions [4].

Figure 2 shows the comparison of total field and Br component fields at the surface of the Moon from SVM [4] and the L1 approach of this study. L1 regularization leads to sparse solutions (where information is concentrated in fewer model parameters). The monopole distribution (black dots) shows that the isolated features on the L1 model fields overlie multiple monopoles and thus are not caused by single point artifacts.

On the other hand, the SVM total field is more spread out (as a result of L2 norm regularization). The Br component of the SVM model has criss-cross pattern and the total field has a few N-S appearing features that may have been caused by external field biases in the vector fields along orbits. Because of these issues, it is worth looking into the characteristics of the data and the different models considered. The range of the downward continued Br field in our high resolution L1 model is <-205, +173> nT, and the range of the SVM Br is <-67, +102> nT. Thus, the LP gradients alone L1 model has greater amplitudes in this local region.

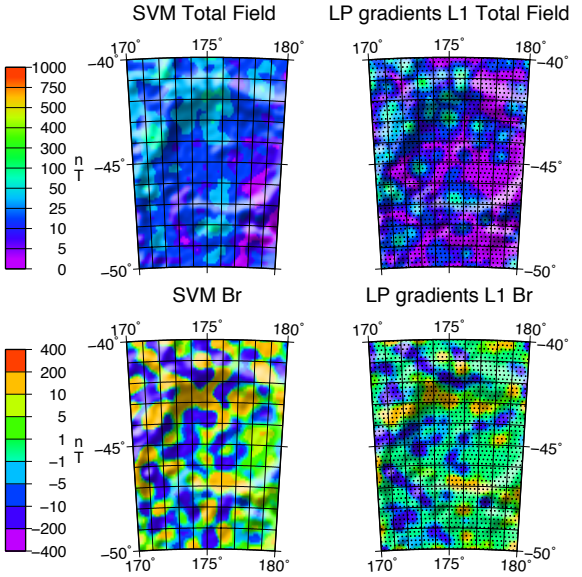

Figure 2. Comparison of total field and Br component fields at the surface of the Moon from the SVM [4] (left) and L1 approach of this study (right) in the region of Von Kármán crater (large depression in shaded relief). Equivalent source locations used in the L1 model are shown by black dots to emphasize that isolated anomaly features are formed over several monopoles and are not associated with instabilities.

Figure 3 shows that along-track differences of the Br component from S/K and LP are consistent with each other. The altitude distribution is however different between the two (see Figure 3 caption). S/K subset has many doublets of very low and high altitude orbits close to each other. It is difficult to deduce the validity of Br components at the surface from gradients at observation altitudes, but the fields appear consistent in their appearance. Although the Br gradients have NW-SE and NE-SW trending features, the criss-cross pattern in the downward continued SVM Br component (Figure 2 left panels) is not obvious in the Br component observed gradients (Figure 3).

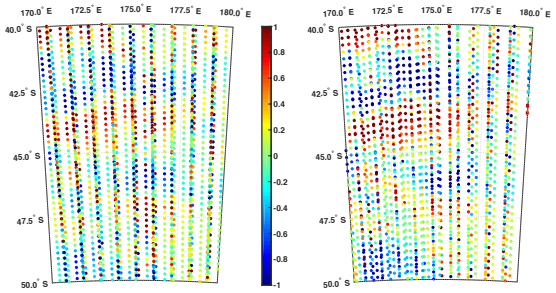

Figure 3. Along-track differences of Br component from SELENE/Kaguya (S/K) (left) and LP (right). Both data show similar features. S/K data in the region have altitude range from 8.7 to 44 km (but have doublets of very low and very high altitude orbits side by side), and their mean altitude and standard deviation are 33 and 11.5 km, respectively. LP data have more uniform altitude range from 20 to 31 km, with the mean and standard deviation of 28 and 3.1 km, respectively.

The Results: We derived global and local high resolution magnetic field models using monopoles [1] with L1 regularization [2]. These models are mathematically sparse, but because the Moon's magnetic field is patchy or localized, they are appropriate for many regions of the Moon. Our highest resolution stable model over the Von Kármán crater in the SPA basin has features consistent with the observed LP along-track gradients and a greater dynamic range than previous high resolution models. Because the surface fields normally have high wavenumber information from shallow sources, which is lost at 20-30 km observation altitude, the fields we observed at satellite altitudes are likely from deeper sources. In particular, the magnetic features do not have a characteristic melt sheet edge effect signature and thus if the melt sheet exists in the crater, the crater was likely formed during a weaker or extinct core field dynamo episode. It would be worthwhile comparing previous space-borne geologic inferences and observations from Chang'E-4 lander/rover [5] with the features observed in the magnetic field of the area and understand the origin of the magnetic fields, especially the NW-SE and NE-SW trending magnetic anomaly features in the region and their absence in the eastern part of Von Kármán crater where Chang'E-4 has landed.

References: [1] O'Brien M. S. and Parker R. L. (1994) *GJI, 118,* 566–578. [2] Olsen N. et al. (2017) *GJI, 211,* 1467–1477. [3] Goossens S. et al. (2018) *LPS XLIX,* Abstract #1645. [4] Tsunakawa et al. (2015) *JGR Planets, 120,* 1160–1185. [5] Huang et al. (2018) *JGR Planets, 123,* 10.1029/2018JE005577.